

Molecular Modeling and Experimental Studies of the Thermodynamic and Transport Properties of Pyridinium-Based Ionic Liquids

Cesar Cadena,[†] Qi Zhao,[‡] Randall Q. Snurr,[‡] and Edward J. Maginn^{*,†}

Department of Chemical and Biomolecular Engineering, University of Notre Dame, Notre Dame, Indiana 46556, and Department of Chemical and Biological Engineering, Northwestern University, Evanston, Illinois 60208

Received: October 29, 2005; In Final Form: December 12, 2005

A combined experimental and molecular dynamics study has been performed on the following pyridinium-based ionic liquids: 1-*n*-hexyl-3-methylpyridinium bis(trifluoromethanesulfonyl)imide ([hmpy][Tf₂N]), 1-*n*-octyl-3-methylpyridinium bis(trifluoromethanesulfonyl)imide ([ompy][Tf₂N]), and 1-*n*-hexyl-3,5-dimethylpyridinium bis(trifluoromethanesulfonyl)imide ([hdmpy][Tf₂N]). Pulsed field gradient nuclear magnetic resonance spectroscopy was used to determine the self-diffusivities of the individual cations and anions as a function of temperature. Experimental self-diffusivities range from 10⁻¹¹ to 10⁻¹⁰ m²/s. Activation energies for diffusion are 44–49 kJ/mol. A classical force field was developed for these compounds, and molecular dynamics simulations were performed to compute dynamic as well as thermodynamic properties. Evidence of glassy dynamics was found, preventing accurate determination of self-diffusivities over molecular dynamics time scales. Volumetric properties such as density, isothermal compressibility, and volumetric expansivity agree well with experiment. Simulated heat capacities are within 2% of experimental values.

Introduction

The study of ionic liquids has experienced tremendous growth in recent years. The fact that these compounds are liquid at ambient temperatures, and that many have immeasurably low vapor pressures and exhibit excellent solvation properties, has sparked a great deal of interest in their use in a wide range of applications including chemical synthesis, separations, lubrication, and catalysis.¹ Ionic liquids can be made from a number of cation classes, including those based on imidazolium, pyrrolidinium, ammonium, phosphonium, guanidinium, and pyridinium. The immense number of ionic liquids that could be made by combining these different cations with a host of potential anions has stimulated work directed at understanding the link between the structure and chemical composition of ionic liquids and their resulting dynamic and thermophysical properties. Without such an understanding, the search for ionic liquids with optimal properties for a given application is a daunting task. There have been many recent studies in which important thermophysical properties have been measured, including volumetric properties,^{2–4} thermal properties,^{5,6} and transport properties.^{3,7,8} Another way this structure–property link has been investigated is through the use of classical condensed phase simulations of pure ionic liquids^{9–19} and their mixtures.^{20–25} In general, the molecular modeling studies have been remarkably successful in determining structural and thermophysical properties. When combined with the experimental work, these studies have enabled researchers to make more informed decisions regarding the properties to be expected for a given class of ionic liquids.

The vast majority of the experimental and modeling work to date has focused on imidazolium-based ionic liquids. As mentioned earlier, however, there are many other potential cation

types that can be used. Pyridinium-based ionic liquids are of particular interest to us, given their potential as a lower cost alternative to imidazolium-based ionic liquids as well as other favorable properties they possess such as an excellent thermal stability.²⁶ Only a handful of experimental studies have been undertaken to measure thermophysical properties for this class of compounds,^{26–29} and we are unaware of any previous molecular modeling work on pyridinium-based ionic liquids.

The present study focuses on the dynamic and volumetric properties of three different ionic liquids all having the same bis(trifluoromethanesulfonyl)imide ([Tf₂N]) anion but the following cations: 1-*n*-hexyl-3-methylpyridinium ([hmpy]), 1-*n*-octyl-3-methylpyridinium ([ompy]), and 1-*n*-hexyl-3,5-dimethylpyridinium ([hdmpy]). Self-diffusivities have been measured for these liquids as a function of temperature. We have also developed a set of classical force field parameters to model these liquids and compared computed dynamics and thermophysical properties to experimental data. The simulations shed light on the local dynamics and structure of these compounds.

Experimental Methodology

Self-Diffusivity Measurements. Pulsed field gradient nuclear magnetic resonance (PFG NMR) is a powerful technique that enables direct determination of the self-diffusivity and has been used recently to examine the dynamics of several imidazolium-based ionic liquids^{30–34} as well as imidazolium-based ionic liquids mixed with alkali halide salts.³⁵ Here, we use the same basic technique to measure the anion and cation self-diffusivities at several temperatures. The following procedures were used to ensure accuracy and reproducibility.

Each ionic liquid was made at Notre Dame and characterized for purity using standard procedures.⁶ Impurity levels of halide (Br⁻) and ammonium ions were measured using an Oakton Ion 510 Series ion meter with Cole-Parmer ion specific probes

[†] University of Notre Dame.

[‡] Northwestern University.

(27502-05 for Br[−], and 27502-03 for NH₄⁺).²⁶ All values were less than 10 ppm for Br[−] and less than 20 ppm for NH₄⁺. Each sample was transferred into a glass NMR tube with an outer diameter of 5 mm (Wilmad 503-PS-8), and the NMR tube was subsequently connected to a vacuum line. The sample was slowly heated to 333 K under a vacuum of 10^{−6} Torr, and then, this condition was held for 2 days in order to remove trace water absorbed in the ionic liquid. Afterward, the sample was slowly cooled to room temperature, and the NMR tube was flame sealed. This preparation significantly reduces the amount of absorbed gases and yields ionic liquids under vacuum.

All PFG NMR measurements were performed at Northwestern University on a Varian INOVA 400 spectrometer equipped with an ultrashielded Doty PFG probe. The stimulated echo pulse sequence with the “longitudinal-eddy-current delay” (LED)^{36,37} was applied to detect the self-diffusivities of the cation (¹H) and anion (¹⁹F) in the ionic liquids. The resonance frequencies of the ¹H and ¹⁹F nuclei were 400.6 and 377.0 MHz, and the corresponding $\pi/2$ pulse widths were about 17.5 and 21 μ s, respectively. Depending on the detected diffusivity, the width and highest intensity of the applied gradient pulse varied in the ranges of 2–3 ms and 90–250 G/cm, respectively. The delay time after the gradient pulse was 30 ms. Measurements of the NMR signals demonstrated that this delay time was long enough to eliminate residual eddy current effects. Thirty-two scans were accumulated, and the diffusion times were about 63 ms. Prior to NMR acquisition at any temperature, the sample was equilibrated for at least 20 min in the probe. The accuracy in temperature was ± 0.1 K. To reduce any experimental artifacts, the intensities and widths of the applied gradient pulses were exactly the same for a given sample for the cation (¹H) and anion (¹⁹F) measurements, though it was demonstrated that the variation of gradient pulse widths and diffusion times had no effect on the reported self-diffusivity. For the cations, the three strongest ¹H peaks were used to obtain the self-diffusivity. The diffusivities measured for these three peaks were averaged to obtain the overall cation diffusivity, and the standard deviation was used to estimate the uncertainty. As a test, the self-diffusivity of fluorobenzene (C₆H₅F) was measured using both its ¹H and ¹⁹F nuclei; at room temperature, the self-diffusivity from ¹H NMR (2.51×10^{-9} m²/s) was consistent with that from the ¹⁹F nuclei (2.50×10^{-9} m²/s), as expected for a single molecular species.

Simulation Methodology

Force Field Parameters. The potential energy of the system was modeled using the following standard functional form

$$\Phi_{\text{tot}} = \sum_{\text{bonds}} k_b(r - r_0)^2 + \sum_{\text{angles}} k_\theta(\theta - \theta_0)^2 + \sum_{\text{dihedrals}} \sum_n k_\chi[1 + \cos(n\chi - \delta)] + \sum_{\text{impropers}} k_\psi(\psi - \psi_0)^2 + \sum_{i=1}^{N-1} \sum_{j>1}^N \left\{ 4\epsilon_{ij} \left[\left(\frac{\sigma_{ij}}{r_{ij}} \right)^{12} - \left(\frac{\sigma_{ij}}{r_{ij}} \right)^6 \right] + \frac{q_i q_j}{r_{ij}} \right\} \quad (1)$$

where the symbols have their usual meaning.³⁸ This class of force fields has been shown in a number of studies^{9,13,16,18,39} to be effective in modeling the thermodynamic properties of imidazolium-based ionic liquids and thus is expected to perform well for pyridinium-based ionic liquids as well. The following procedures were used to develop appropriate parameters for eq 1. Coulombic and Lennard-Jones interactions were neglected for atom pairs separated by less than three bonds. For atoms

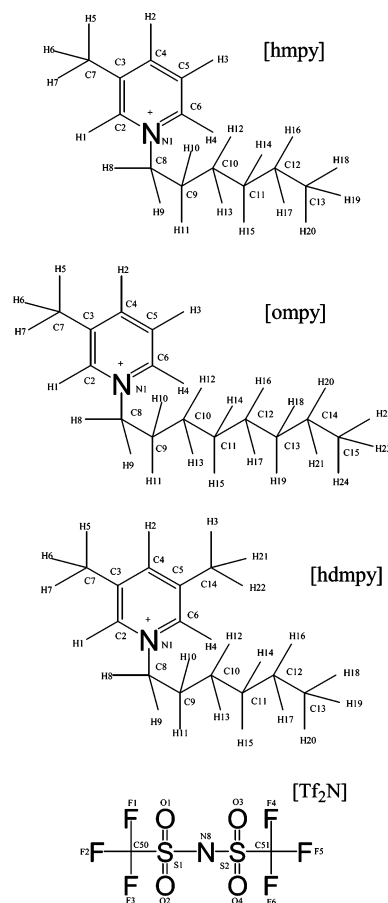


Figure 1. Atom labels of pyridinium cations and the [Tf₂N] anion.

separated by three bonds, Coulombic interactions were scaled by 50% for the cation. To be consistent with the anion force field,¹⁷ both Coulombic and Lennard-Jones interactions for atoms separated by three bonds were scaled by 50% for the anion. Full Lennard-Jones and Coulombic potential terms were used for all other interactions. The following switching function was applied to the Lennard-Jones interactions

$$S_{\text{vdw}}(|\vec{r}_{ij}|) = \begin{cases} 1 & \text{if } |\vec{r}_{ij}| \leq r_s \\ (r_c^2 - |\vec{r}_{ij}|^2)^2(r_c^2 + 2|\vec{r}_{ij}|^2 - 3r_s^2)/(r_c^2 - r_s^2)^3 & \text{if } r_s < |\vec{r}_{ij}| \leq r_c \\ 0 & \text{if } r_c \leq |\vec{r}_{ij}| \end{cases} \quad (2)$$

where the cutoff (r_c) was 12 Å and the onset distance (r_s) was 10.5 Å. Nominal bond lengths and bond angles were obtained from ab initio calculations of the separate ions using Gaussian 03⁴⁰ at the B3LYP-6311-G* level of theory. The CHELPG⁴¹ algorithm was applied to the cations in order to determine partial charges. Parameters for the [Tf₂N] anion were taken from the literature.¹⁷ A frequency analysis was carried out on the isolated cations and anion optimized structures to obtain the ideal gas heat capacities. The rest of the parameters and force constants were extracted from the similarities found in the CHARMM⁴² potential for oxidized nicotinimide and from our previous work involving imidazolium-based ionic liquids.² All of the force field parameters along with the detailed nomenclature of the investigated systems are tabulated in the Supporting Information. Figure 1 shows the labeling of the atoms for the pyridinium cations and the [Tf₂N] anion. As described below, the initial parameter set (“FF1”) resulted in densities that were slightly

higher than the experimental values. To correct this, a second parametrization ("FF2") was thus developed by increasing the Lennard-Jones diameters of all of the atoms in the cation ring (C, N, and H) by 15%.

Simulation Details. Molecular dynamics simulations in several ensembles were run using the program NAMD.⁴³ Electrostatics were handled by means of a particle-mesh Ewald method^{44,45} with a grid size of 48 Å per side. Whenever pressure and/or temperature were to be controlled, Langevin dynamics with a Nosé–Hoover barostat/thermostat was applied. The barostat oscillation time and damping factors were set to 1 ps. The thermostat damping factor was set at 5 ps⁻¹. A multiple time step algorithm was used with a 1 fs reference time step. Full electrostatics was evaluated every 4 fs, while short-range nonbonded terms were computed every 2 fs. The following procedure was used to prepare well-equilibrated initial configurations. Two hundred fifty formula units (ion pairs) of each of the ionic liquids were randomly placed in a low-density cubic box with periodic boundary conditions. Antibumping constraints were used to prevent ions from overlapping. Then, a standard conjugate gradient energy minimization procedure was applied to relax the system. Next, the density of the system was equilibrated by carrying out a 1 ns isobaric–isothermal (NPT) simulation. Following this, a 1 ns canonical (NVT) simulation was conducted. Finally, microcanonical ensemble runs were performed for 5.5 ns. All of these runs were made at temperatures ranging from 298 to 348 K in 10 K increments as well as temperatures of 373, 398, and 423 K. The last 5 ns of the NVE simulations were utilized as production data; for the rest of the ensembles, the last 500 ps of the trajectory were used to compute the properties relevant for the particular ensemble. Snapshots were written every 1 ps for the NVE simulations and every 0.1 ps for the rest of the simulations. Additional NPT simulations were conducted at pressures of 500, 1000, 2000, and 5000 bar for 1 ns at 298 K. For the cohesive energy density calculations, the ideal gas state was modeled by simulating a single formula unit in an unbounded box in the canonical ensemble.

Results and Discussion

Pure Liquid Thermodynamic Quantities. The following approach was taken to compute the thermophysical properties of the pure ionic liquids. The volumetric expansivity is defined as

$$\alpha_p = \frac{1}{\langle V \rangle} \left(\frac{\partial \langle V \rangle}{\partial T} \right)_p = \frac{1}{\langle V \rangle k_B T^2} (\langle V \hat{H} \rangle - \langle V \rangle \langle \hat{H} \rangle) \quad (3)$$

where \hat{H} is the configurational enthalpy, $\hat{H} = \Phi + PV$. We chose to split the total potential energy into two terms, $\Phi = \Phi^{\text{NB}} + \Phi^{\text{INT}}$, where Φ^{NB} includes all intermolecular as well as intramolecular nonbonded terms (Lennard-Jones and Coulombic) and Φ^{INT} includes all intramolecular bonded terms (bond stretching, angle bending, dihedral, and improper torsion). The isothermal compressibility is given by

$$\kappa_T = -\frac{1}{\langle V \rangle} \left(\frac{\partial \langle V \rangle}{\partial P} \right)_T = \frac{1}{\langle V \rangle k_B T^2} (\langle V^2 \rangle - \langle V \rangle^2) \quad (4)$$

The volumetric expansivity and isothermal compressibility were computed via finite difference estimation from a series of NPT simulations; use of the fluctuation formulas in eqs 3 and 4 resulted in values having a very large statistical uncertainty.

The heat capacity at constant pressure, defined as

$$C_p(T, P) = \left(\frac{\partial \langle H \rangle}{\partial T} \right)_p \quad (5)$$

was calculated in the following manner.⁴⁶ The enthalpy, $H = \Phi^{\text{NB}} + \Phi^{\text{INT}} + K + PV$, was split into ideal gas and residual terms according to $\langle H \rangle = \langle H^{\text{ig}} \rangle + \langle H^{\text{res}} \rangle$, where $H^{\text{ig}} = \Phi^{\text{INT}} + K + Nk_B T$ and $H^{\text{res}} = \Phi^{\text{NB}} + PV - Nk_B T$. The heat capacity can thus be written as $C_p(T, P) = C_p^{\text{ig}}(T) + C_p^{\text{res}}(T, P)$, where

$$C_p^{\text{ig}}(T, P) = \left(\frac{\partial \langle H^{\text{ig}} \rangle}{\partial T} \right)_p \quad (6)$$

$$C_p^{\text{res}}(T, P) = \left(\frac{\partial \langle H^{\text{res}} \rangle}{\partial T} \right)_p \quad (7)$$

In principle, both contributions to the heat capacity can be computed from a molecular dynamics (MD) simulation. In practice, however, it is more common for the residual contribution to the heat capacity to be determined from a classical simulation and the ideal gas contribution to be obtained from experiment. Since experimental ideal gas heat capacities are not available for ionic liquids, we chose to compute the ideal gas heat capacity from a frequency analysis of the optimized cation and anion structures obtained from the ab initio calculations. The ideal gas heat capacity computed from the classical force field was significantly higher than that obtained from the ab initio calculations, which suggests that the intramolecular force field parameters may need additional refinement. The residual heat capacity was computed by carrying out nine independent NPT simulations at temperatures ranging from 298 to 423 K. The residual enthalpy was then fit to a straight line and the residual heat capacity determined from eq 7. Thus, the computed heat capacities are an average over 298–423 K.

The cohesive energy density (c) was computed from knowledge of the liquid density and the internal energy difference between an ideal gas ion pair and the average internal energy of an ion pair in the liquid phase. Densities were determined from the average molar volume obtained from the NPT simulations.

Figure 2 shows the experimental and computed densities for each ionic liquid plotted as a function of temperature. Simulated densities are displayed in circles for FF1 and squares for FF2. As can be seen, both parametrizations obtain the correct relative densities, with [hmpy][Tf₂N] being most dense and [ompy][Tf₂N] being least dense. However, FF1 clearly overestimates the density by anywhere from 1 to 5%. To improve upon this, the collision diameters of the ring atoms (N, C, and H) were increased by 15%. This set of parameters, denoted FF2, does a much better job of matching the experimental densities.

As discussed below, there is evidence that these liquids have glasslike dynamics at lower temperatures. Consequently, densities and other static properties may be expected to show history dependence. To check for this, six independent NPT simulations starting from different low-density initial configurations were run for [ompy][Tf₂N] at 298 K and [hmpy][Tf₂N] at 318 and 328 K using FF1. The standard deviations of these densities were small, ranging from 0.001 to 0.004 g/cm³. This indicates that the equilibration procedure generates reproducible results but does not necessarily guarantee that thermodynamic equilibrium has been achieved. That is, local glassy minima could be quenched by this procedure. The density-versus-temperature plot for [hmpy][Tf₂N] (Figure 2c) seems to indicate this as the slope changes between 310 and 340 K. To further test this,

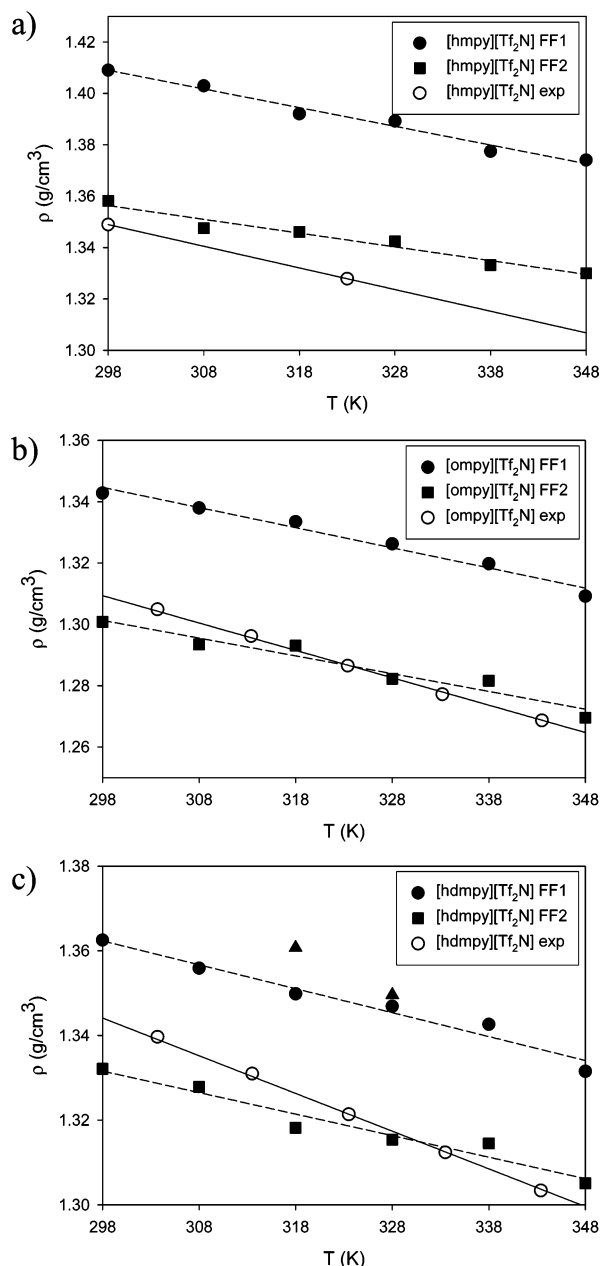


Figure 2. Experimental and simulation densities for pyridinium-based ionic liquids. In part c, triangles correspond to the average of six simulations started from configurations at ± 10 K (see text).

the [hdmpy][Tf₂N] configurations from the six 318 K simulations were heated to 328 K and run for an additional 1 ns, while the six 328 K configurations were cooled to 318 K and also run for an additional 1 ns. Figure 2c shows that in both cases the density increased relative to the previous results at these temperatures, with the 318 K system showing the largest increase of more than 0.01 g/cm³. These new densities, labeled as triangles in Figure 2c, appear to follow the slope of the high-temperature data. This result suggests glassy behavior below 328 K and that properties computed below this temperature may suffer from nonergodicity.

Table 1 lists computed and (when available) experimental values for the volumetric expansivity, isothermal compressibility, and heat capacity. The computed volumetric expansivities for both FF1 and FF2 are slightly lower than the experimental values, ranging from 4×10^{-4} to 5×10^{-4} K⁻¹, while the experimental values²⁶ range from 6×10^{-4} to 7×10^{-4} K⁻¹.

TABLE 1: Volumetric Expansivity, Isothermal Compressibility, and Heat Capacity of Each Ionic Liquid^a

IL	$\alpha_{\text{exp}}(\text{K}^{-1}) \times 10^4$	$\alpha^b(\text{K}^{-1}) \times 10^4$	$\alpha^c(\text{K}^{-1}) \times 10^4$	$\kappa_T^b(\text{bar}^{-1}) \times 10^5$
[hmpy][Tf ₂ N]	6.35 ₁	5.23 ₃₈	3.99 ₄₃	1.84 ₂₁
[ompy][Tf ₂ N]	6.94 ₂	4.95 ₃₉	4.51 ₅₈	1.97 ₂₂
[hdmpy][Tf ₂ N]	6.74 ₂	4.02 ₈₀	3.85 ₄₆	1.93 ₂₃

IL	$C_{P,\text{exptl}}(\text{J/K mol})$	$C_P^b(\text{J/K mol})$	$C_P^{\text{ig}}(\text{J/K mol})$	$C_P^{\text{res}}(\text{J/K mol})$
[hmpy][Tf ₂ N]	634	637 ₆	448	189 ₆
[ompy][Tf ₂ N]	681	686 ₈	489	197 ₈
[hdmpy][Tf ₂ N]	642.5	661 ₇	474	187 ₇

^a The experimental volumetric expansivity results are unpublished;²⁹ the experimental heat capacities are from Crosthwaite et al.²⁶ and are the average of values at 298 and 323 K. Uncertainties in all tables are indicated by subscripts, for example, $5.23_{38} = 5.23 \pm 0.38$. ^b FF1. ^c FF2.

TABLE 2: Simulated Cohesive Energy Densities (c , J/cm³) of Pyridinium-Based Ionic Liquids

T (K)	[hmpy][Tf ₂ N]	[ompy][Tf ₂ N]	[hdmpy][Tf ₂ N]
298	549 ₆₂	513 ₅₅	503 ₅₅
308	533 ₆₁	504 ₅₆	491 ₅₆
318	542 ₆₃	505 ₅₉	483 ₅₆
328	538 ₆₆	507 ₆₁	492 ₅₈
338	532 ₆₈	481 ₅₉	490 ₆₁
348	541 ₇₀	483 ₅₉	489 ₆₁

Interestingly, if one considers the two highest temperature results and the recomputed densities shown as triangles in Figure 2c, then the estimated volumetric expansivity is $(7.02 \pm 0.44) \times 10^{-4}$ K⁻¹, which agrees very well with the experimental value of 6.74×10^{-4} K⁻¹. This rather large variation in the simulated volumetric expansivity demonstrates the difficulty involved in computing properties in the glassy regime of these materials and suggests that the errors reported in Table 1 (which were obtained from the standard error of a least-squares fit) are probably too low. This is a common problem in the simulation of glasslike materials, where the system is easily trapped in different local minima. Isothermal compressibilities computed with FF1 are just under 2×10^{-5} bar⁻¹, while experimental values⁴⁷ for [hmpy][Tf₂N] and [hdmpy][Tf₂N] are found to be on the order of 3×10^{-5} bar⁻¹. This is similar to the isothermal compressibility of various imidazolium-based ionic liquids.⁴ The general conclusion that may be drawn from these results is that the three systems show the same tendency to expand/contract under the influence of temperature and pressure, and thus, the intermolecular forces among the various ions are similar. This is not surprising, given the structural similarities among the three liquids as well as the prominent role electrostatics plays in the volumetric properties of these liquids.

The computed heat capacities are in excellent agreement with experiment. The simulations correctly capture the experimental trend that [ompy][Tf₂N] has the highest heat capacity, followed by [hdmpy][Tf₂N], with [hmpy][Tf₂N] having the lowest heat capacity. The longer the length of the alkyl chain or more substitution along the ring (i.e., the higher the molecular weight), the more energy storage mechanisms the cation has, and thus the higher the heat capacity.

The cohesive energy density is an important quantity that has been used to predict solubility trends in ionic liquids with the help of regular solution theory.⁴⁸ Table 2 lists computed values of the cohesive energy density for each compound as a function of temperature. The calculations indicate that cohesive energy densities are on the order of 500–550 J/cm³, with the value decreasing slightly as the alkyl chain length and substitu-

tion along the ring increases. There is also a slight decrease observed as temperature increases, although all of these trends are modest, especially considering the uncertainty in the calculations. Interestingly, the computed values for these ionic liquids are significantly lower than the previously computed values for 1-*n*-butyl-3-methylimidazolium hexafluorophosphate.^{9,11} The larger [Tf₂N] anion appears to lower the cohesive energy density (and thus the solubility parameter) when compared to the smaller [PF₆] anion. It is difficult to measure cohesive energy densities experimentally, although estimates have been made through various means. Swiderski and co-workers⁴⁹ estimated cohesive energy densities for a range of ionic liquids using a Kamlet–Taft model and the rate of a Diels–Alder reaction. They determined the cohesive energy density for 1-*n*-butyl-2,3-dimethylimidazolium [Tf₂N] to be 586 J/cm³, while 1-*n*-butyl-3-methylimidazolium [Tf₂N] had an estimated cohesive energy density of 620 J/cm³, both of which are consistent with the values computed here. This group also observed a decrease in cohesive energy density with the addition of a methyl group to the imidazolium ring and as smaller anions such as [PF₆] were replaced by bigger anions such as [Tf₂N]. This is consistent with calculations here and elsewhere.^{9,11} The same trend was also observed by Camper and co-workers,⁵⁰ who used the lattice energy of different ionic liquids to estimate heats of vaporization and thus cohesive energy densities. They observed that small anions such as [BF₄] and [PF₆] have larger cohesive energy densities than [Tf₂N], although their estimated values were about 2–3 times higher than those computed here as well as those estimated by Swiderski and co-workers. Taken together, these results provide some guidance as to how one might tailor the solubility of different species through the addition of alkyl groups to the cation ring as well as changes to the anion.

Liquid Structure. Various site–site radial distribution functions (RDFs) were computed to obtain insight into the organization of the liquid. Figure 3 shows the center-of-mass RDFs for cation–cation, anion–anion, and cation–anion interactions. All three liquids exhibit a first cation–anion peak at approximately 5 Å and broad cation–cation/anion–anion peaks at 8–9 Å. The first cation–anion peak for [ompy][Tf₂N] is broader and less intense than in the case of the other two systems, which is most likely due to the additional conformational flexibility of the longer alkyl chain causing the location of the cation center of mass to be more diffuse. The systems all exhibit long-range spatial correlations that extend beyond 2 nm, a feature that has been observed experimentally^{19,51–53} as well as in simulations^{11,13,18,39} of other ionic liquid systems.

Figure 4 shows the number integrals ($N(r)$) for cation–anion centers of mass. The results are similar for each liquid; in all cases, an ion is singly coordinated with a counterion at about 5.2 Å. Beyond this distance, there are subtle differences in the coordination pattern. If the first solvation shell is defined to be the first minimum in the cation–anion RDF, which occurs at roughly 8.5 Å, then there are approximately five counterions coordinating with each ion. [ompy][Tf₂N] has a slightly lower coordination from 5 to 8 Å, which again is consistent with the larger size of its cation.

Additional insight into the organization of the liquid can be obtained from calculating different site–site distribution functions. Parts a and b of Figure 5 show the RDFs for the N1 and C4 sites, respectively, in the [ompy] ring with the N, S, and O atoms in the [Tf₂N] anion. Atom label definitions are provided in Figure 1. The distributions for the other cations are similar. The first observation that can be made is that the O1 atom is

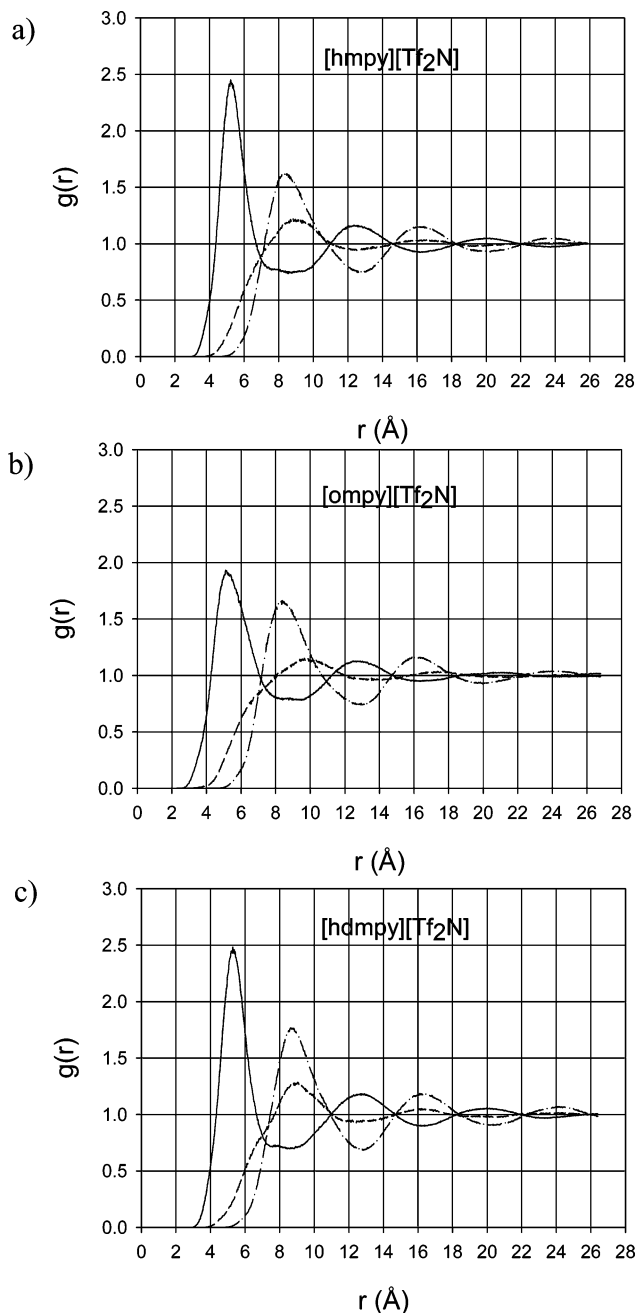


Figure 3. Radial distributions for the centers of mass of pyridinium-based materials. Solid lines, +/–; dashed lines, +/+; dash–dotted lines, –/–.

closest to the cation center of mass, followed by the S1 atom and then the N8 atom. This indicates that the nominally linear [Tf₂N] anion is “bent” with the electronegative oxygen atoms closely associating with the cation. One can observe a secondary peak for the O1 atom at about 6 Å; this arises due to configurations in which the equivalent O2 atom interacts with the cation. A similar weak shoulder exists for S1.

To determine if the anion preferentially locates near certain regions of the cation, we computed the probability distribution for the angles formed between the plane of the cation ring and the plane formed by the S1–N8–S2 atoms of the anion. The resulting distribution was uniform, indicating no preferred spatial orientation of the anion about the cation. In other words, while the [Tf₂N] anion is bent, it is located uniformly about the cation and does not associate with one particular site of the ring.

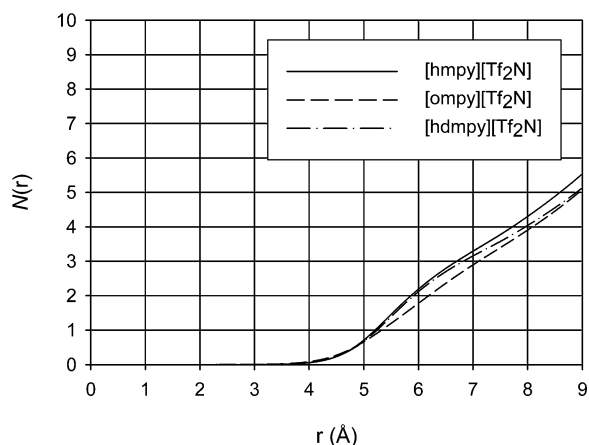


Figure 4. Cation-anion center-of-mass number integrals for pyridinium-based ionic liquids.

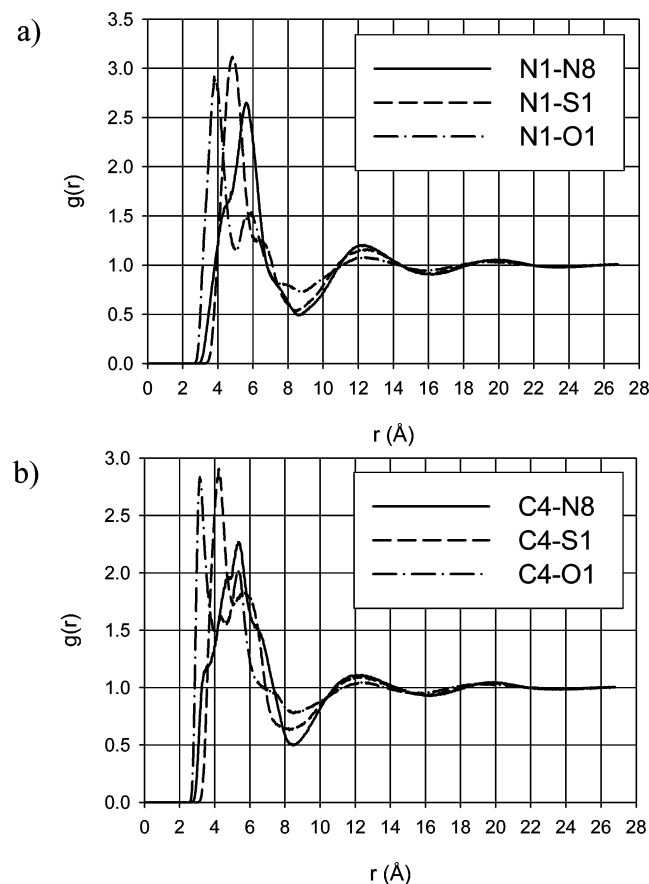


Figure 5. Radial distribution functions for N1 (a) and C4 (b) sites in the [ompy] cation with nitrogen, sulfur, and oxygen atoms in the [Tf₂N] anion.

Dynamic Properties. The microscopic dynamics of ionic liquids plays a critical role in determining the rheological properties of these compounds. It also governs mass transfer behavior, which is crucial in determining chemical reactivity in ionic liquid solvents and the performance of ionic liquids in separations and electrochemical applications. A particularly useful measure of liquid dynamics that is amenable to both experimental and computational determination is the self-diffusivity (D_s) defined as

$$D_s \equiv \frac{1}{6} \lim_{t \rightarrow \infty} \frac{d}{dt} \langle |\vec{r}(t) - \vec{r}(0)|^2 \rangle \quad (8)$$

where the term in pointed brackets is the mean-squared

TABLE 3: PFG NMR and Simulated Self-Diffusivities ($\times 10^{11} \text{ m}^2/\text{s}$) for Pyridinium-Based Ionic Liquids^a

T (°C)	$^{19}\text{F}_{\text{exptl}}$	$^1\text{H}_{\text{exptl}}$ (Avg)	$\text{anion}_{\text{sim}}$	$\text{cation}_{\text{sim}}$
[hmpy][Tf₂N]				
25	1.207	1.218 ₀₀₅	0.083 ₀₀₈	0.108 ₀₀₆
35	2.122	2.145 ₀₁₃	0.175 ₀₁₁	0.197 ₀₁₂
45	3.415	3.448 ₀₁₇	0.280 ₀₂₁	0.329 ₀₀₉
55	5.544	5.596 ₀₄₂	0.214 ₀₃₃	0.277 ₀₄₉
65	9.658	9.613 ₀₈₈	0.446 ₀₃₅	0.493 ₀₂₁
75	17.690	17.867 ₁₉₇	0.624 ₀₃₅	0.672 ₀₂₀
100			1.546 ₀₂₉	1.445 ₀₂₂
125			3.200 ₀₉₇	3.644 ₀₇₄
150			6.216 ₂₀₆	6.721 ₂₃₅
[ompy][Tf₂N]				
25	0.916	0.861 ₀₀₄	0.149 ₀₁₀	0.144 ₀₁₄
35	1.659	1.555 ₀₂₃	0.171 ₀₂₈	0.186 ₀₂₂
45	2.713	2.539 ₀₂₅	0.217 ₀₂₂	0.256 ₀₁₄
55	4.302	4.011 ₀₂₃	0.343 ₀₁₂	0.325 ₀₄₇
65	7.158	6.731 ₀₃₇	0.424 ₀₄₁	0.557 ₀₂₈
75	12.400	11.707 ₁₂₁	0.617 ₀₆₄	0.631 ₀₁₉
100			1.225 ₀₄₃	1.277 ₀₅₉
125			2.623 ₀₆₉	3.255 ₀₃₉
150			5.648 ₃₂₆	5.781 ₂₂₇
[hdmpy][Tf₂N]				
25	0.980	0.925 ₀₀₇	0.127 ₀₁₅	0.118 ₀₁₅
35	1.804	1.674 ₀₀₉	0.195 ₀₁₉	0.202 ₀₁₆
45	3.017	2.844 ₀₁₀	0.186 ₀₄₅	0.228 ₀₂₅
55	5.163	4.867 ₀₇₆	0.230 ₀₁₅	0.268 ₀₁₉
65	8.847	8.450 ₁₁₉	0.383 ₀₁₇	0.380 ₀₁₇
75	17.130	17.090 ₂₈₈	0.505 ₀₄₉	0.590 ₀₃₅
100			1.381 ₀₅₃	1.381 ₀₅₈
125			2.596 ₀₈₇	2.697 ₁₇₃
150			6.859 ₂₁₅	6.599 ₃₆₆

^a Note that, as discussed in the text, simulation results have not attained diffusive behavior and should be considered “apparent” self-diffusivities indicative of subdiffusive motion.

displacement (MSD) of an individual ion. Previous PFG NMR studies of imidazolium-based ionic liquids^{30–34} found that the cation has a slightly higher self-diffusivity than the anion, despite its larger size. These studies also found that the self-diffusivity correlates well with the inverse of the viscosity, but application of the Stokes–Einstein model yields ion sizes that are not qualitatively correct.

We have determined self-diffusivities for the anions and cations of each liquid as a function of temperature using PFG NMR and have also attempted to compute the self-diffusivity using molecular dynamics. Table 3 lists the measured and computed values. Two main observations can be made from the experimental data.

First, the experimental self-diffusivities of the cations and anions are similar for each ionic liquid and are on the order of $1 \times 10^{-11} \text{ m}^2/\text{s}$ at room temperature. This is roughly 2 orders of magnitude smaller than that of water.⁵⁴ [hmpy][Tf₂N] has the highest self-diffusivity, while [ompy][Tf₂N] has the lowest, with [hdmpy][Tf₂N] falling between these two. This trend is consistent with the molar volumes and viscosities; the higher the molar volume and lower the viscosity of the liquid, the higher the self-diffusivity.

Second, for [hmpy][Tf₂N], the cation has a slightly higher self-diffusivity than the anion at nearly all temperatures, although given the uncertainty in the data this difference is not statistically significant. For the other two ionic liquids, the *anion* clearly has the larger self-diffusivity. The bulky [ompy] cation has the lowest self-diffusivity at all temperatures, while [hdmpy] has a self-diffusivity midway between [ompy] and [hmpy]. As noted above, previous PFG NMR studies of imidazolium-based ionic liquids always found that the cations had larger self-diffusivities

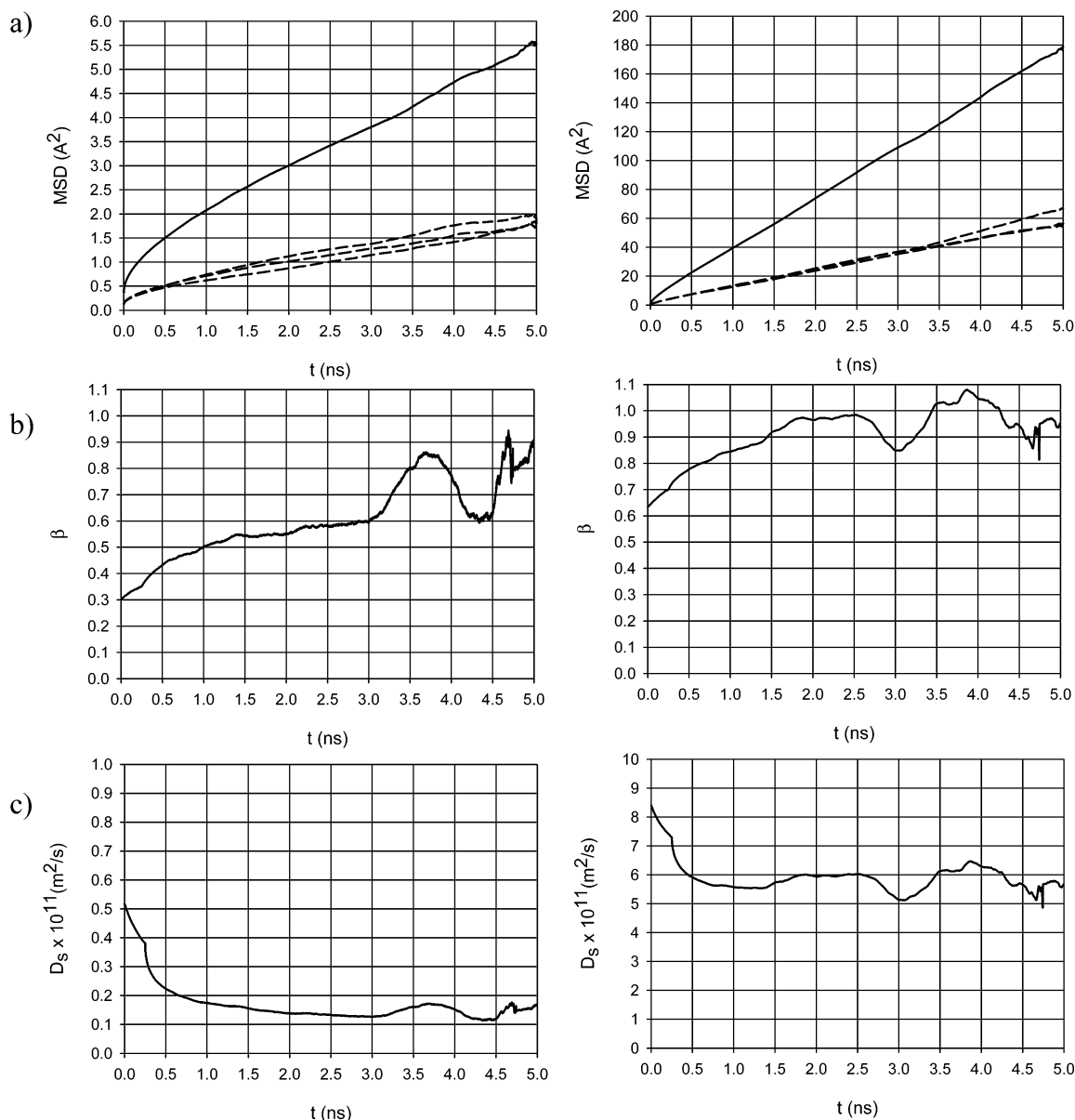


Figure 6. Diffusion analysis of the cation in [ompy][Tf₂N] at low and high temperatures (left, 298 K; right, 423 K): (a) mean-squared displacement; (b) β ; (c) apparent self-diffusivity computed over varying time intervals.

than their smaller anion pairs. The present results suggest that this is not a universal phenomenon but that the nature of the ions themselves is important in determining the relationship between cation and anion self-diffusivities. Increasing alkyl substitution and chain length apparently serves to hinder cation diffusion in these systems such that the anions now diffuse faster than the cations. It is interesting to note, however, that anion diffusivities do track cation diffusivities. That is, the [Tf₂N] anion has the highest self-diffusivity when paired with the fastest diffusing [hmpy] cation and the lowest self-diffusivity when paired with the slowest diffusing [ompy] cation. These results follow the trend that is expected with molar volume and also suggest that there is ion pairing present in the liquid such that ions do not exhibit free diffusion but rather travel in pairs or clusters.

To gain additional insight into the operative diffusion mechanisms, eq 8 was applied to the results of the microcanonical ensemble molecular dynamics simulations to attempt to compute the self-diffusivity. It is important to note that eq 8 is valid only when true diffusive motion is observed. For the

PFG NMR experiments, the diffusion times over which data were taken were very long (63 ms), so that diffusional motion was assured. Such long times are not attainable with molecular dynamics, however, so great care must be taken to ensure that true diffusive processes are simulated. Figure 6a shows the MSD as a function of time for [ompy][Tf₂N] at 298 and 423 K. The solid line is the total MSD, while the dashed lines are for displacements along the three Cartesian directions. These latter values give an indication of the statistical variation in the MSD and also confirm that there is no preferential diffusion along a given Cartesian axis. Both plots appear to show linear behavior at long times, and on the basis of this, one would be tempted to directly apply eq 8 to compute D_s . Upon closer inspection of the results, however, one finds that neither system is clearly in the diffusive regime, particularly in the 298 K case.

The dynamic nature of a liquid can be characterized by examining the way in which the mean-squared displacement scales with time. This can be quantified⁵⁵ as

$$\langle |\vec{r}(t) - \vec{r}(0)|^2 \rangle = \Delta r^2 \propto t^\beta \quad (9)$$

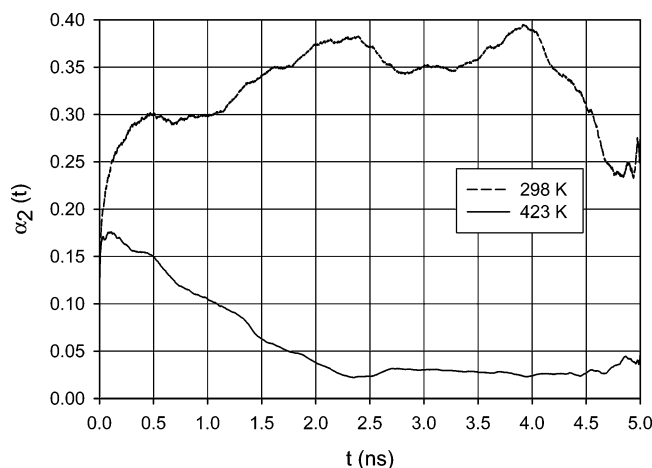


Figure 7. $\alpha_2(t)$ behavior at low and high temperatures for the cation in [ompy][Tf₂N].

where β characterizes the type of motion present in the system. At very short times when ballistic motion dominates, $\beta = 2$. For long-time diffusive motion, eq 8 implies $\beta = 1$. At intermediate time scales, however, subdiffusive dynamics characteristic of glasslike behavior can result in $\beta < 1$, a situation observed previously with ionic liquids.³⁹ By plotting the following expression as a function of time

$$\beta(t) = \frac{d \log(\Delta r^2)}{d \log(t)} \quad (10)$$

one can easily determine which dynamic regime a system is in. Figure 6b shows a running average of $\beta(t)$ at 298 K calculated using a window of ± 250 ps. It is clear that the system has not yet reached diffusive behavior even after 5 ns, although, at the highest temperature, the system does approach diffusive behavior. Note that the apparent self-diffusivities depend strongly upon the time interval over which the MSD is taken. Figure 6c shows the running average of the apparent D_s as a function of time over which the MSD is averaged. At 298 K, where the system exhibits glassy dynamics, the apparent self-diffusivity drops rapidly by nearly an order of magnitude when the averaging is extended beyond a few hundred picoseconds. Beyond about 2 ns, the apparent value of D_s is insensitive to the time over which the MSD is averaged, but the results in Figure 6b clearly indicate that this is not the true self-diffusivity. At 423 K, the apparent self-diffusivity also drops and stabilizes to a consistent value after about 2 ns, but one should also be cautious of this value as well, given the behavior of β .

An alternative means for assessing whether a system exhibits true diffusive behavior^{39,55} is to calculate a so-called non-Gaussian parameter⁵⁶ given by

$$\alpha_2(t) = \frac{3\langle |\Delta r(t)|^4 \rangle}{5\langle |\Delta r(t)|^2 \rangle^2} - 1 \quad (11)$$

$\alpha_2(t)$ will approach zero as diffusive behavior is reached but will be nonzero during short-time ballistic or subdiffusive motion.⁵⁷ Figure 7 shows $\alpha_2(t)$ for [omim] at 298 and 423 K. Similar behavior is observed for the other two ionic liquids. At the lower temperature, $\alpha_2(t)$ is nonzero even after 20 ns (not shown). At the higher temperature, $\alpha_2(t)$ approaches zero, but at a very slow rate. These results, along with the power-law dependence of the MSD with time, suggest that an accurate

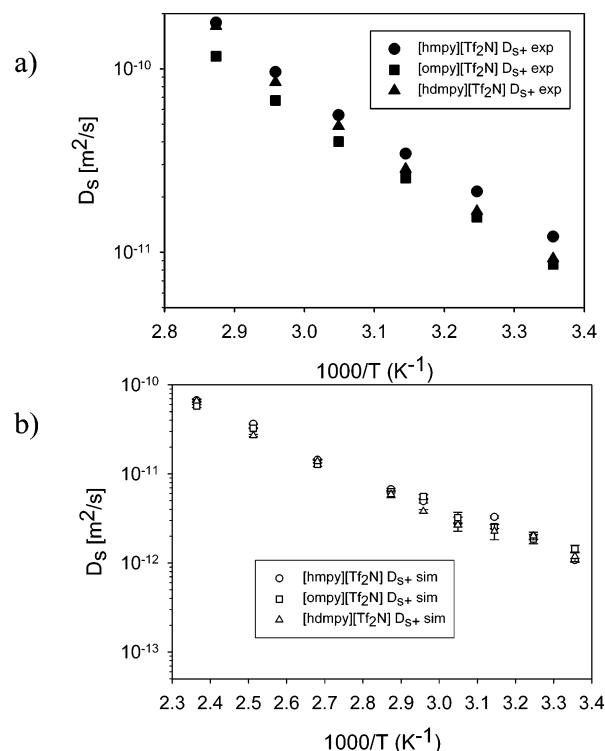


Figure 8. Experimental (a) and computed (b) self-diffusivity temperature dependence of cations. Note that, as discussed in the text, the simulations are not long enough to observe true diffusive behavior, so the results in part b are “apparent” self-diffusivities.

self-diffusivity cannot be determined at 298 K without extraordinarily long simulations. Even at 423 K, very long simulations of greater than 5 ns are needed to reliably estimate the self-diffusivity. Interestingly, if one were to estimate the self-diffusivity using only the first few hundred picoseconds of a simulation, Figure 6c suggests that the (erroneous) computed value would be much closer to the experimental value than what is estimated from the long-time behavior observed here. We note that all of the dynamic simulations were carried out using FF1. Since this force field gives densities that are about 4% too high, part of the discrepancy between experiment and simulation could be due to this. To test this, we carried out simulations at 298 and 348 K for all three ionic liquids using the same protocol as that used to compute the self-diffusivity with FF1, except FF2 was used. Within the uncertainty of the results, the FF2 apparent self-diffusivities were essentially unchanged from the FF1 values at 298 K and were actually slightly lower at 348 K. Thus, we do not believe the large differences between the experimental and simulated self-diffusivities are due to inaccurate densities. We also note that Yan and co-workers⁵⁸ have reported that the use of a polarizable model increases the self-diffusivity by a factor of 3 relative to a fixed charge model in simulations of 1-ethyl-3-methylimidazolium nitrate at 400 K. This is due to the fact that the polarizable model enables an additional screening mechanism to be operative, thereby reducing the “cage” effect that tends to trap ions in their local environment. It is very likely that such a mechanism could be responsible for some of the underestimation of the dynamics for this system, and thus, a polarizable model would be expected to yield slightly faster dynamics than the present fixed charge model. We do not expect this to account for all of the differences between simulations and experiments. Rather, it appears that the simulations are still only capturing the subdiffusive regime ($\beta < 1$) and that true

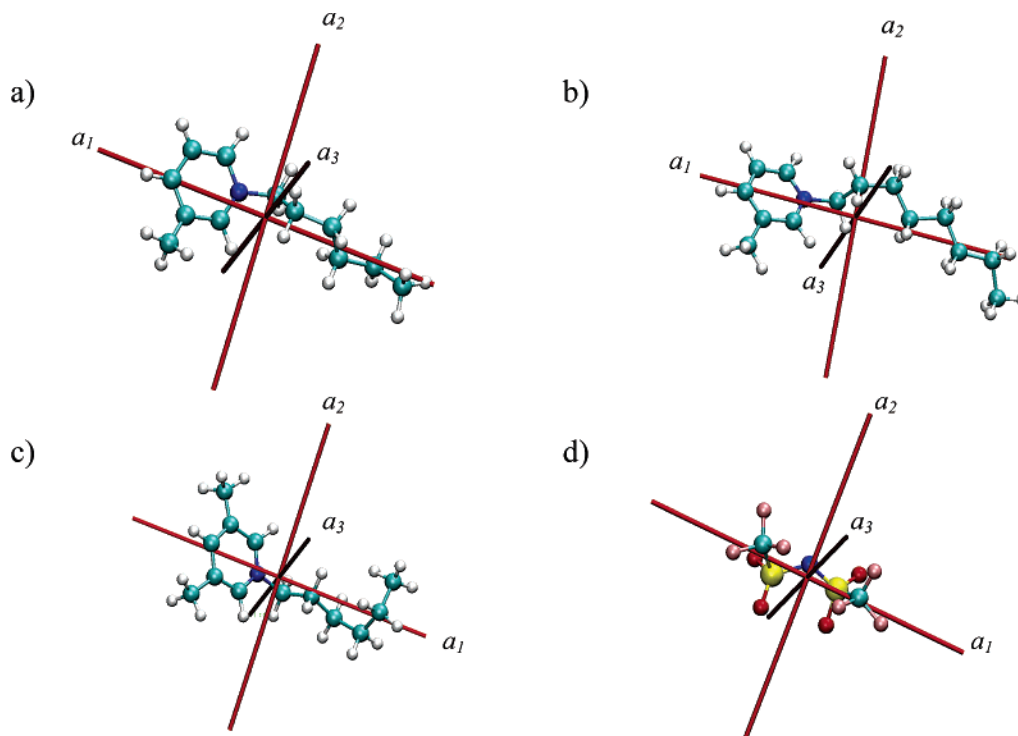


Figure 9. Principal axes of the species studied in this work (a_1 , long axis; a_2 , intermediate axis; a_3 , short axis): (a) [hmmpy]⁺; (b) [ompy]⁺; (c) [hdmpy]⁺; (d) [Tf₂N]⁻.

diffusive behavior for these systems will only occur over much larger time scales. There are several results that support this line of reasoning.

Previous studies reported that ionic liquid self-diffusivities do not show Arrhenius behavior and instead diffusivities had to be fit to a Vogel–Tamman–Fulcher model.³¹ However, both the experimental data and simulation results from the present study do follow a simple Arrhenius model, as shown in Figure 8. The experimental activation energy for diffusion was found to be about 44–49 kJ/mol, while the simulations predict a more modest value of 31–35 kJ/mol. Some of this difference could again be due to the neglect of polarization effects, but a more likely explanation is that the simulations are only probing local motion within a glasslike matrix. This type of motion should have a lower activation energy than translational motion, which is what is observed in the simulations.

We can also examine rotational dynamics to gain additional insight. The principal axes of both the cation and anion were determined every 0.1 ps by means of an atomic mass weighted covariance matrix⁵⁹

$$s_{jk} = \frac{\sum_{i=1}^n m_i (q_{ij} - \langle q \rangle_j) (q_{ik} - \langle q \rangle_k)}{\sum_{i=1}^n m_i} \quad (12)$$

where s_{jk} is the weighted covariance between the j th and k th atomic coordinates, n is the number of atoms in the ion, m_i is the atomic mass of the i th atom, q_{ij} and q_{ik} represent the j th and k th coordinate ($j, k = x, y, z$) of the i th atom, respectively, and $\langle q \rangle$ is the corresponding average value.

The eigenvectors of s correspond to the principal axes of the ion. The eigenvalues or principal moments of inertia are well separated, allowing for the unambiguous assignment of the three axes. The smallest eigenvalues range from 0.2 to 0.9, the

intermediate eigenvalues range from 0.9 to 1.5, and the largest eigenvalues are between 3.5 and 20. Figure 9 shows the principal axis for all of the species studied in this work, where a_1 is the long axis, a_2 the intermediate axis, and a_3 the short axis. For each cation, the long axis points along the alkyl chain and through the pyridinium ring. The intermediate axis a_2 is in the plane of the pyridinium ring, while the short axis a_3 is normal to the plane of the ring. For the anion, the long axis is roughly along the C–S–N–S–C backbone, as expected. The intermediate axis is in the plane of the S–N–S bond angle, and the short axis is normal to this plane. This analysis suggests that the cations and anions will experience slow rotational motion around the a_3 axis (slow decorrelation of a_1) and relatively rapid rotation about the a_1 axis.

To quantify the rotational dynamics, we define a correlation function, $C(t)$, as⁶⁰

$$C(t) = \left\langle \frac{1}{2} [3 \cos^2 \theta_i(t) - 1] \right\rangle \quad (13)$$

where $\theta_i(t)$ defines the orientation angle of the principal axis i as a function of time. Figure 10 shows the behavior of $C(t)$ for the long axis of each ion at 348 K. As expected, the smaller anion rotates faster than any of the cations. In addition, the rotational behavior of the anion is essentially independent of the cation that it is paired with. For the cations, [ompy] exhibits the slowest long-axis rotation, which is understandable, since it has the longest alkyl chain. The other two cations appear to show similar long-axis rotation behavior.

A better comparison can be made by calculating a rotational time constant, τ_i , via the following expression

$$\tau_i = \int_0^\infty C(t) dt \approx \frac{\int_0^{t_0} C(t) dt}{1 - C(t_0)} \quad (14)$$

where we have assumed that $C(t)$ decays as a pure exponential beyond time $t = t_0$.

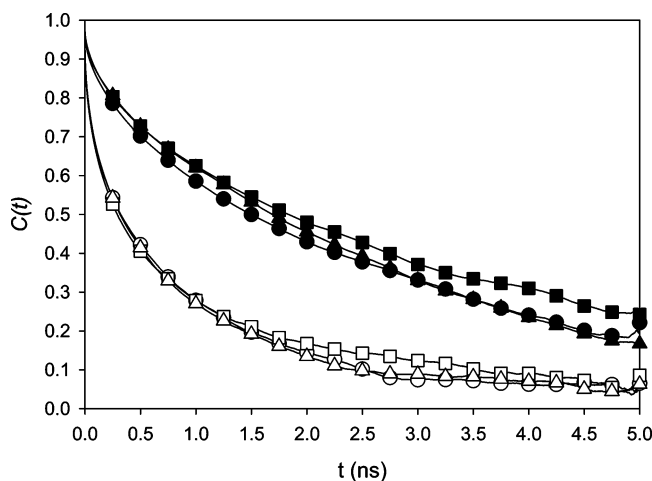


Figure 10. $C(t)$ behavior of pyridinium ionic liquids (cations, closed symbols; anions, open symbols): (circles) [hmpy][Tf₂N]; (squares) [ompy][Tf₂N]; (triangles) [hdmpy][Tf₂N].

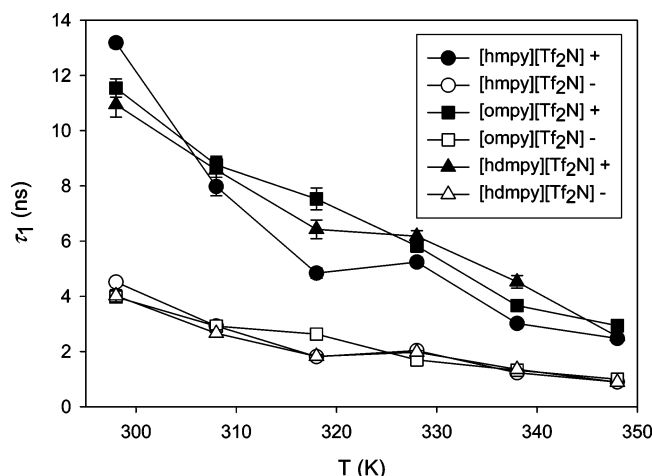


Figure 11. Rotational time constants for the long axis of pyridinium-based ionic liquids.

Figure 11 shows a plot of τ_1 for each cation and anion as a function of temperature. Table 4 lists all of the time constants for each species at all of the temperatures simulated. The results show that there is a strong temperature dependence for the long-axis rotation time, particularly for the cations. Consistent with our observation of the “glasslike” dynamics of the system at low temperature, the rotational time constant of the cations is greater than 10 ns at room temperature. Even the anions have a 4 ns decorrelation time, indicating that diffusive motion will not be observed in simulations of less than this time. Interestingly, τ_2 and τ_3 are roughly equal for each ion at every temperature. There is a very large difference between these rotational times and τ_1 at low temperature, particularly with the cations. The ratio of τ_1 to $(\tau_2 + \tau_3)/2$ drops from roughly 4.0 for [ompy] at 298 K to less than 3.5 at 348 K. A similar drop in this ratio is seen for [hmpy]. For the anions, this ratio is roughly 2–2.5 and nearly independent of temperature. This is a strong signature of a transition from glasslike dynamics at low temperature driven mainly by the slow, nonuniform rotational motion of the cations to “liquidlike” dynamics at higher temperatures. An indication of this transition can also be seen in the plateau region in Figure 11 for the cation τ_1 . All of these observations are consistent with the diffusion results discussed earlier. Thus, we cannot expect to obtain true self-diffusion behavior from a simulation shorter than the longest τ_1 value. On the basis of this, the computed self-diffusivities in

TABLE 4: Rotational Time Constants (in ns) for the Principal Axes of the Cations and Anions in the Ionic Liquids

T (K)	τ_3	τ_2	τ_1	τ_3	τ_2	τ_1
[hmpy]⁺						
298	3.534 ₂₀₂	3.257 ₁₆₂	13.183 ₁₇₆	2.149 ₁₁₄	1.746 ₀₇₆	4.513 ₀₅₈
308	2.395 ₁₅₆	2.289 ₁₄₆	7.973 ₃₃₆	1.407 ₀₈₃	1.051 ₀₆₀	2.923 ₁₆₉
318	1.639 ₁₀₂	1.491 ₀₇₆	4.837 ₁₈₈	1.049 ₀₄₃	0.757 ₀₂₃	1.811 ₀₂₂
328	1.617 ₀₇₁	1.521 ₀₆₈	5.239 ₁₇₁	1.134 ₀₆₅	0.727 ₀₁₉	2.032 ₁₁₄
338	0.986 ₀₃₁	0.931 ₀₃₁	3.013 ₀₆₅	0.661 ₀₂₂	0.446 ₀₀₈	1.225 ₀₄₀
348	0.860 ₀₂₉	0.780 ₀₂₁	2.471 ₀₂₉	0.568 ₀₃₆	0.315 ₀₀₂	0.893 ₀₃₃
[ompy]⁺						
298	2.997 ₁₃₅	2.660 ₁₂₄	11.541 ₃₃₂	1.939 ₁₂₇	1.532 ₀₈₀	3.974 ₀₉₂
308	2.302 ₁₅₉	2.053 ₁₃₁	8.759 ₃₁₆	1.682 ₁₁₆	1.219 ₀₆₅	2.917 ₁₃₆
318	1.968 ₁₂₁	1.737 ₀₈₂	7.527 ₃₉₇	1.373 ₀₉₄	1.032 ₀₅₃	2.627 ₁₅₄
328	1.534 ₁₄₆	1.389 ₁₃₀	5.822 ₁₃₉	1.057 ₀₇₆	0.760 ₀₃₇	1.696 ₀₆₂
338	1.168 ₀₅₂	1.046 ₀₆₃	3.663 ₁₀₂	0.759 ₀₃₅	0.509 ₀₁₇	1.319 ₀₅₉
348	0.904 ₀₄₅	0.795 ₀₃₃	2.934 ₀₈₁	0.598 ₀₃₁	0.386 ₀₀₈	0.992 ₀₃₂
[hdmpy]⁺						
298	4.781 ₁₈₆	4.519 ₁₇₄	10.947 ₄₅₇	1.838 ₁₃₂	1.561 ₀₉₄	4.017 ₂₂₁
308	3.289 ₁₉₈	2.972 ₁₇₃	8.580 ₄₃₄	1.439 ₀₈₃	1.058 ₀₅₁	2.656 ₁₂₈
318	2.479 ₁₀₇	2.356 ₀₉₃	6.425 ₃₃₇	1.026 ₀₄₁	0.743 ₀₃₀	1.823 ₀₆₆
328	2.310 ₀₈₂	2.277 ₀₈₀	6.172 ₂₀₀	1.059 ₀₆₉	0.758 ₀₃₃	1.973 ₀₆₀
338	1.754 ₀₅₇	1.798 ₀₆₄	4.522 ₂₃₀	0.804 ₀₃₇	0.522 ₀₀₈	1.351 ₀₀₉
348	1.115 ₀₀₂	1.097 ₀₀₆	2.543 ₀₁₀	0.550 ₀₂₈	0.325 ₀₀₄	0.885 ₀₂₃
[Tf₂N]⁻						

Table 3 are expected to be lower than the actual values, which is in fact observed.

The principal axis analysis yields information on the conformations adopted by the cations and anions. Of particular interest is the [Tf₂N]⁻ anion, which can exhibit dihedral rotations about the S–N and C–S bonds. As noted, the long axis is about the anion backbone, but the C–S–N–S torsion distribution is smooth and centered about 125°. We do not observe a fully extended trans state (180°), which is consistent with the radial distribution finding that the anion exists in a bent state.

Finally, Urahata and Ribeiro⁶¹ have recently investigated the difference in dynamics between cations and anions using molecular dynamics simulations. They found that while roughly “spherical” anions such as [PF₆]⁻ and [BF₄]⁻ exhibit homogeneous diffusion tendencies, alkyl-imidazolium cations exhibit a kind of “diffusional anisotropy”, with diffusion in a direction along the plane of the ring and perpendicular to the main alkyl chain being preferred over other directions. This explains why these cations have larger self-diffusivities than the anions. Such an analysis was not performed here, although it is interesting to note that a nonzero value for $\alpha_2(t)$ is a strong indication of a system with dynamic heterogeneity,^{39,55} which is expected to lead to the type of diffusional anisotropy Urahata and Ribeiro observed.

Conclusions

Dynamic and thermophysical properties of ionic liquids comprised of three different pyridinium-based cations paired with the bis(trifluoromethanesulfonyl)imide anion have been determined through a combined experimental and molecular modeling study. Self-diffusivities were measured for each ionic liquid as a function of temperature using pulsed field gradient nuclear magnetic resonance spectroscopy. The self-diffusivities were found to range from 10⁻¹¹ to 10⁻¹⁰ m²/s, with an apparent activation energy of about 44–49 kJ/mol. Cation and anion self-diffusivities were similar for 1-*n*-hexyl-3-methylpyridinium bis(trifluoromethanesulfonyl)imide, while the anion showed a slightly higher diffusivity than the cation for 1-*n*-hexyl-3,5-dimethylpyridinium bis(trifluoromethanesulfonyl)imide and 1-*n*-octyl-3-methylpyridinium bis(trifluoromethanesulfonyl)imide. This is in contrast to previous NMR studies of imidazolium-

based ionic liquids, in which the cation was found to have a higher self-diffusivity than the anion. Self-diffusivities decreased as the molecular weight of the cation increased.

Molecular modeling studies were also carried out on these systems to compute both dynamic and thermophysical properties. Force field parameters were developed for these ionic liquids, and the computed density, heat capacity, isothermal compressibility, and volumetric expansivity all agreed well with experiment. The cohesive energy density was also computed, but experimental data for this property do not exist. The liquids were found to exhibit long-range order, similar to other ionic liquids. Each cation has a coordination sphere of roughly five anions.

It was not possible to reliably compute self-diffusivities, even for simulations as long as 20 ns, due to sluggish glasslike dynamical behavior. Long-axis rotational time constants were found to be on the order of 4 ns for [Tf₂N] and 11–13 ns for the pyridinium cations at 298 K. These times decrease to around 1 and 3 ns at 348 K. To obtain a self-diffusivity, simulations need to be conducted over longer time scales than these. Apparent self-diffusivities computed from the simulations show a strong dependence on the time over which the mean-squared displacement was monitored. At the longest times, the systems still exhibited subdiffusive motion, resulting in apparent self-diffusivities that were roughly 10 times lower than experimental values. Self-diffusivity results obtained from previous molecular simulation studies in which much shorter time scales were probed should be re-examined in light of the present findings.

Acknowledgment. This work was financially supported by the U.S. Air Force Office of Scientific Research (F49620-03-1-0212) and by the Chemical Sciences, Geosciences and Biosciences Division, Office of Basic Energy Sciences, U.S. Department of Energy (DE-FG02-03ER15457). We thank Dr. Mark Muldoon for providing the pyridinium-based ionic liquid samples.

Supporting Information Available: A complete listing of the force field parameters used in this work. This material is available free of charge via the Internet at <http://pubs.acs.org>.

References and Notes

- (1) Marsh, K. N.; Boxall, J. A.; Lichtenthaler, R. *Fluid Phase Equilib.* **2004**, *219*, 93.
- (2) Cadena, C.; Anthony, J. L.; Shah, J. K.; Morrow, T. I.; Brennecke, J. F.; Maginn, E. J. *J. Am. Chem. Soc.* **2004**, *126*, 5300.
- (3) Dzyuba, S. V.; Bartsch, R. A. *ChemPhysChem* **2002**, *3*, 161.
- (4) Gu, Z. Y.; Brennecke, J. F. *J. Chem. Eng. Data* **2002**, *47*, 339.
- (5) Van Valkenburg, M. E.; Vaughn, R. L.; Williams, M.; Wilkes, J. S. *Thermochim. Acta* **2005**, *425*, 181.
- (6) Fredlake, C. P.; Crosthwaite, J. M.; Hert, D. G.; Aki, S. N. V. K.; Brennecke, J. F. *J. Chem. Eng. Data* **2004**, *49*, 954.
- (7) Seddon, K. R.; Stark, A.; Torres, M. J. *Pure Appl. Chem.* **2000**, *72*, 2275.
- (8) Seddon, K. R.; Stark, A.; Torres, M. J. *ACS Symp. Ser.* **2002**, *819*, 34.
- (9) Morrow, T. I.; Maginn, E. J. *J. Phys. Chem. B* **2002**, *106*, 12807.
- (10) Morrow, T. I.; Maginn, E. J. *J. Phys. Chem. B* **2003**, *107*, 9160.
- (11) Shah, J. K.; Brennecke, J. F.; Maginn, E. J. *Green Chem.* **2002**, *4*, 112.
- (12) Margulis, C. J. *Mol. Phys.* **2004**, *102*, 829.
- (13) Margulis, C. J.; Stern, H. A.; Berne, B. J. *J. Phys. Chem. B* **2002**, *106*, 12017.
- (14) Liu, Z. P.; Huang, S. P.; Wang, W. C. *J. Phys. Chem. B* **2004**, *108*, 12978.
- (15) Lopes, J. N. C.; Deschamps, J.; Padua, A. A. H. *J. Phys. Chem. B* **2004**, *108*, 11250.
- (16) Lopes, J. N. C.; Deschamps, J.; Padua, A. A. H. *J. Phys. Chem. B* **2004**, *108*, 2038.
- (17) Lopes, J. N. C.; Padua, A. A. H. *J. Phys. Chem. B* **2004**, *108*, 16893.
- (18) Hanke, C. G.; Price, S. L.; Lynden-Bell, R. M. *Mol. Phys.* **2001**, *99*, 801.
- (19) de Andrade, J.; Boes, E. S.; Stassen, H. *J. Phys. Chem. B* **2002**, *106*, 3546.
- (20) Hanke, C. G.; Atamas, N. A.; Lynden-Bell, R. M. *Green Chem.* **2002**, *4*, 107.
- (21) Hanke, C. G.; Johansson, A.; Harper, J. B.; Lynden-Bell, R. M. *Chem. Phys. Lett.* **2003**, *374*, 85.
- (22) Hanke, C. G.; Lynden-Bell, R. M. *J. Phys. Chem. B* **2003**, *107*, 10873.
- (23) Lynden-Bell, R. M.; Atamas, N. A.; Vasilyuk, A.; Hanke, C. G. *Mol. Phys.* **2002**, *100*, 3225.
- (24) Shah, J. K.; Maginn, E. J. *Fluid Phase Equilib.* **2004**, *222*, 195.
- (25) Shah, J. K.; Maginn, E. J. *J. Phys. Chem. B* **2005**, *109*, 10395.
- (26) Crosthwaite, J. M.; Muldoon, M. J.; Dixon, J. K.; Anderson, J. L.; Brennecke, J. F. *J. Chem. Thermodyn.* **2005**, *37*, 559.
- (27) Carrera, G.; Aires-de-Sousa, J. *Green Chem.* **2005**, *7*, 20.
- (28) Docherty, K. M.; Kulpa, C. F. *Green Chem.* **2005**, *7*, 185.
- (29) Brennecke, J. F. Personal communication, 2005.
- (30) Every, H. A.; Bishop, A. G.; MacFarlane, D. R.; Oradd, G.; Forsyth, M. *Phys. Chem. Chem. Phys.* **2004**, *6*, 1758.
- (31) Noda, A.; Hayamizu, K.; Watanabe, M. *J. Phys. Chem. B* **2001**, *105*, 4603.
- (32) Tokuda, H.; Hayamizu, K.; Ishii, K.; Susan, M. A. B. H.; Watanabe, M. *J. Phys. Chem. B* **2005**, *109*, 6103.
- (33) Umecky, T.; Kanakubo, M.; Ikushima, Y. *J. Mol. Liq.* **2005**, *119*, 77.
- (34) Umecky, T.; Kanakubo, M.; Ikushima, Y. *Fluid Phase Equilib.* **2005**, *228*, 329.
- (35) Hayamizu, K.; Aihara, Y.; Nakagawa, H.; Nukuda, T.; Price, W. S. *J. Phys. Chem. B* **2004**, *108*, 19527.
- (36) Gibbs, S. J.; Johnson, C. S. *J. Magn. Reson.* **1991**, *93*, 395.
- (37) Wu, D. H.; Chen, A. D.; Johnson, C. S. *J. Magn. Reson., Ser. A* **1995**, *115*, 260.
- (38) Allen, M. P.; Tildesley, D. J. *Computer Simulations of Liquids*; Clarendon: Oxford, U.K., 1987.
- (39) Del Popolo, M. G.; Voth, G. A. *J. Phys. Chem. B* **2004**, *108*, 1744.
- (40) Frisch, M. J.; Trucks, G. W.; Schlegel, H. B.; Scuseria, G. E.; Robb, M. A.; Cheeseman, J. R.; Montgomery, J. A., Jr.; Vreven, T.; Kudin, K. N.; Burant, J. C.; Millam, J. M.; Iyengar, S. S.; Tomasi, J.; Barone, V.; Mennucci, B.; Cossi, M.; Scalmani, G.; Rega, N.; Petersson, G. A.; Nakatsuji, H.; Hada, M.; Ehara, M.; Toyota, K.; Fukuda, R.; Hasegawa, J.; Ishida, M.; Nakajima, T.; Honda, Y.; Kitao, O.; Nakai, H.; Klene, M.; Li, X.; Knox, J. E.; Hratchian, H. P.; Cross, J. B.; Bakken, V.; Adamo, C.; Jaramillo, J.; Gomperts, R.; Stratmann, R. E.; Yazyev, O.; Austin, A. J.; Cammi, R.; Pomelli, C.; Ochterski, J. W.; Ayala, P. Y.; Morokuma, K.; Voth, G. A.; Salvador, P.; Dannenberg, J. J.; Zakrzewski, V. G.; Dapprich, S.; Daniels, A. D.; Strain, M. C.; Farkas, O.; Malick, D. K.; Rabuck, A. D.; Raghavachari, K.; Foresman, J. B.; Ortiz, J. V.; Cui, Q.; Baboul, A. G.; Clifford, S.; Cioslowski, J.; Stefanov, B. B.; Liu, G.; Liashenko, A.; Piskorz, P.; Komaromi, I.; Martin, R. L.; Fox, D. J.; Keith, T.; Al-Laham, M. A.; Peng, C. Y.; Nanayakkara, A.; Challacombe, M.; Gill, P. M. W.; Johnson, B.; Chen, W.; Wong, M. W.; Gonzalez, C.; Pople, J. A. *Gaussian 03*, revision C.02; Gaussian, Inc.: Wallingford, CT, 2004.
- (41) Breneman, C. M.; Wiberg, K. B. *J. Comput. Chem.* **1990**, *11*, 361.
- (42) Mackerell, A. D.; Wiorkiewicz-Kuczera, J.; Karplus, M. *J. Am. Chem. Soc.* **1995**, *117*, 11946.
- (43) Kale, L.; Skeel, R.; Bhandarkar, M.; Brunner, R.; Gursoy, A.; Krawetz, N.; Phillips, J.; Shinozaki, A.; Varadarajan, K.; Schulten, K. *J. Comput. Phys.* **1999**, *151*, 283.
- (44) Darden, T.; York, D.; Pedersen, L. *J. Chem. Phys.* **1993**, *98*, 10089.
- (45) Essmann, U.; Perera, L.; Berkowitz, M. L.; Darden, T.; Lee, H.; Pedersen, L. G. *J. Chem. Phys.* **1995**, *103*, 8577.
- (46) Lagache, M.; Ungerer, P.; Boutin, A.; Fuchs, A. H. *Phys. Chem. Chem. Phys.* **2001**, *3*, 4333.
- (47) Grubb, G.; Hert, D.; Aki, N. V. K. S.; Brennecke, J. F. Manuscript in preparation, 2005.
- (48) Scovazzo, P.; Camper, D.; Kieft, J.; Poshusta, J.; Koval, C.; Noble, R. *Ind. Eng. Chem. Res.* **2004**, *43*, 6855.
- (49) Swiderski, K.; McLean, A.; Gordon, C. M.; Vaughan, D. H. *Chem. Commun.* **2004**, 2178.
- (50) Camper, D.; Becker, C.; Koval, C.; Noble, R. *Ind. Eng. Chem. Res.* **2005**, *44*, 1928.
- (51) Takahashi, S.; Suzuya, K.; Kohara, S.; Koura, N.; Curtiss, L. A.; Saboungi, M. L. *Z. Phys. Chem.: Int. J. Res. Phys. Chem. Chem. Phys.* **1999**, *209*, 209.
- (52) Hardacre, C.; Holbrey, J. D.; McMath, S. E. J.; Bowron, D. T.; Soper, A. K. *J. Chem. Phys.* **2003**, *118*, 273.
- (53) Hardacre, C.; McMath, S. E. J.; Nieuwenhuyzen, M.; Bowron, D. T.; Soper, A. K. *J. Phys.: Condens. Matter* **2003**, *15*, S159.
- (54) Hertz, H. G.; Franks, F. *Water, A Comprehensive Treatise*; Plenum Press: New York, 1973; Vol. 3.
- (55) Qian, J.; Hentschke, R.; Heuer, A. *J. Chem. Phys.* **1999**, *110*, 4514.

- (56) Rahman, A. *Phys. Rev.* **1964**, *136*, A405.
- (57) vanMegen, W.; Underwood, S. M.; Muller, J.; Mortensen, T. C.; Henderson, S. I.; Harland, J. L.; Francis, P. *Prog. Theor. Phys. Suppl.* **1997**, *171*.
- (58) Yan, T. Y.; Burnham, C. J.; Del Popolo, M. G.; Voth, G. A. *J. Phys. Chem. B* **2004**, *108*, 11877.
- (59) Todeschini, R.; Consonni, V. *Methods and Principles in Medicinal Chemistry*; Wiley-VCH: Berlin, 2000; Vol. 11.
- (60) McQuarrie, D. A. *Statistical Mechanics*; University Science Books: Sausalito, CA, 2000.
- (61) Urahata, S. M.; Ribeiro, M. C. C. *J. Chem. Phys.* **2005**, *122*, 024511.